Inorganic Chemistry

Article

pubs.acs.org/IC

PPh_3-Derivatives of $[Pt_{3n}(CO)_{6n}]^{2-}$ (n = 2−6) Chini's Clusters: Syntheses, Structures, and ^{31}P NMR Studies

Iacopo Ciabatti, Cristina Femoni, Maria Carmela Iapalucci, Giuliano Longoni, Tatiana Lovato, and Stefano Zacchini*

Dipartimento di Chimica Industriale "Toso Montanari", Università di Bologna, Viale Risorgimento 4-40136 Bologna, Italy

Supporting Information

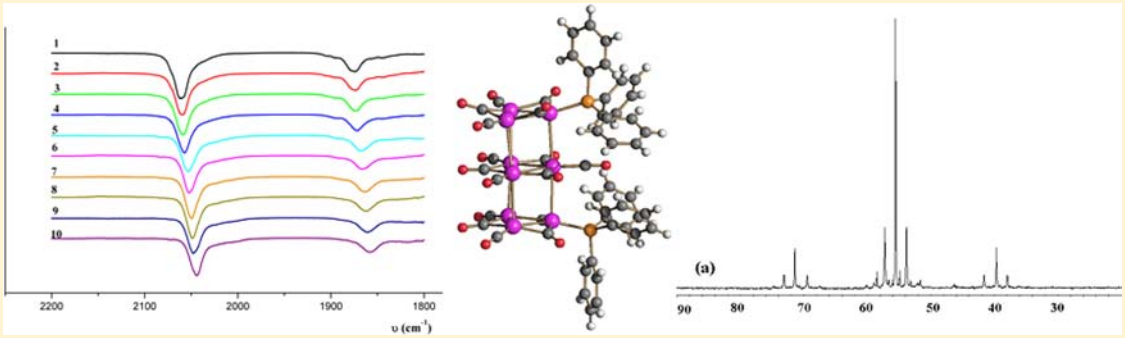

ABSTRACT: The reaction of the $[Pt_{3n}(CO)_{6n}]^{2-}$ (n = 2−6) Chini's clusters with increasing amounts of PPh_3 has been investigated in detail by combined FT-IR, $^{31}P\{^1H\}$ NMR, and electrospray ionization-mass spectrometry (ESI-MS) studies, showing that up to three CO ligands are gradually substituted by PPh_3, resulting in isonuclear phosphine-substituted anionic clusters of general formula $[Pt_{3n}(CO)_{6n-x}(PPh_3)_x]^{2-}$ (n = 2−6; x = 1−3). Further addition of PPh_3 results in the elimination of the neutral $Pt_3(CO)_3(PPh_3)_3$ species and formation of lower nuclearity anionic clusters. $[Pt_{12}(CO)_{22}(PPh_3)_2]^{2-}$ and $[Pt_9(CO)_{16}(PPh_3)_2]^{2-}$ have been structurally characterized, and they maintain the trigonal prismatic structures of the parent homoleptic clusters, with the two PPh_3 ligands bonded to different external Pt_3-triangles in relative cis-position. Conversely, the crystal structure of $[Pt_6(CO)_{10}(PPh_3)_2]^{2-}$ shows that its metal cage is transformed from trigonal prismatic to trigonal antiprismatic after CO/PPh_3 exchange.

1. INTRODUCTION

Countless examples of homoleptic and heteroleptic metal clusters stabilized by phosphine ligands are known, in which the metal displays an oxidation state close to zero.[1] Focusing our attention on heteroleptic PR_3/CO clusters of Group 10 metals, the most notable examples are the Pd/CO/PR_3 clusters, which include several species with nuclearities ranging from 10 to 165.[2] It is noticeable that these heteroleptic Pd clusters may reach very high nuclearities, even if no homoleptic Pd/CO cluster is known. In addition, it must be remarked that most of the species reported to date are neutral and only six examples of anionic Pd/CO/PR_3 clusters are known.[3,4]

On the contrary, the chemistry of Pt/CO/PR_3 clusters is not as developed as that for the Pd-analogues, even if richer than Ni. It mostly includes low nuclearity species such as $Pt_3(CO)_3(PR_3)_3$, $Pt_3(CO)_3(PR_3)_4$, $Pt_4(CO)_5(PR_3)_4$, $Pt_5(CO)_6(PR_3)_4$, and $Pt_6(CO)_6(dppm)_3$,[5] as well as a few larger neutral clusters.[6,7] Besides, some cationic species have been reported,[8] whereas no anionic Pt/CO/PR_3 cluster is known. This is contrasted by the fact that several homoleptic anionic Pt/CO clusters are known.[9−14]

To fill this gap, we decided to reinvestigate the reaction of $[Pt_{3n}(CO)_{6n}]^{2-}$ (n = 2−6) with PPh_3. These clusters show a very interesting structure (Figure 1), composed by the stacking of triangular $Pt_3(\mu\text{-}CO)_3(CO)_3$ units along a common C_3 axis and arranged in a nearly eclipsed fashion, resulting in a trigonal prismatic geometry.[9] Interestingly, these molecular clusters may form in the solid state infinite chains morphologically and functionally resembling molecular metal wires.[10] Their self-assembly has been exploited for applications in electronics and as printable metals.[15,16]

It has been previously reported that addition of PPh_3 to $[Pt_{3n}(CO)_{6n}]^{2-}$ (n = 2−6) results in the elimination of $Pt_3(\mu\text{-}CO)_3(PPh_3)_3$ and formation of lower nuclearity $[Pt_{3(n-1)}(CO)_{6(n-1)}]^{2-}$ species.[9] Supposing that these reactions might proceed initially via the gradual substitution of up to three CO ligands with PPh_3 followed by inter-triangular Pt−Pt bond cleavage and elimination of $Pt_3(\mu\text{-}CO)_3(PPh_3)_3$, we decided to reinvestigate the above reaction by stepwise addition of PPh_3 to $[Pt_{3n}(CO)_{6n}]^{2-}$ (n = 2−6) and monitoring the reaction via IR, $^{31}P\{^1H\}$ NMR spectroscopy, and ESI-MS. Competition between CO substitution and metal−metal bond

Received: November 20, 2012
Published: March 26, 2013

   dx.doi.org/10.1021/ic3025414 | Inorg. Chem. 2013, 52, 4384−4395

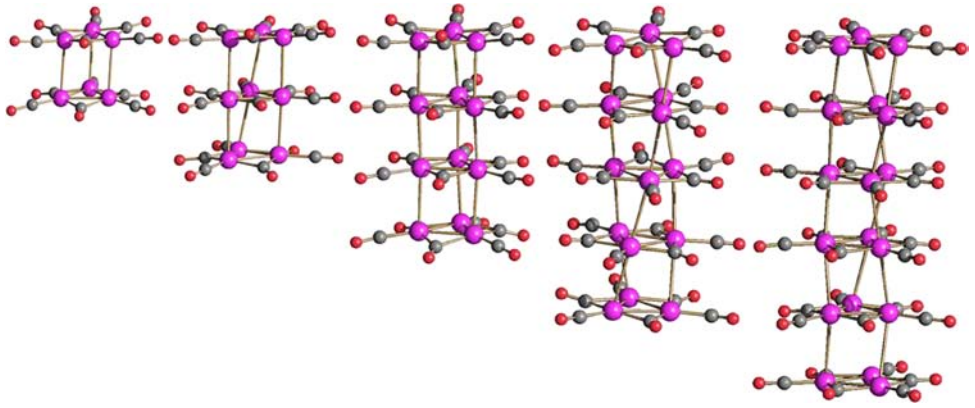

Figure 1. Molecular structures of the $[Pt_{3n}(CO)_{6n}]^{2-}$ (n = 2−6) clusters.

cleavage is indeed a general problem in the chemistry of carbonyl clusters, especially for lighter transition metals.[1,17−20]

This allowed the preparation of several anionic phosphine derivatives of the Chini's clusters, among which $[Pt_{12}(CO)_{22}(PPh_3)_2]^{2-}$, $[Pt_9(CO)_{16}(PPh_3)_2]^{2-}$, and $[Pt_6(CO)_{10}(PPh_3)_2]^{2-}$ have been structurally characterized via X-ray crystallography. The nature of all other species present in solution at different stages of the reaction have been recognized and formulated by combined FT-IR, ESI-MS, and $^{31}P\{^1H\}$ NMR spectroscopy studies.

2. RESULTS AND DISCUSSION

2.1. Synthesis and Spectroscopic Characterization of $[Pt_{12}(CO)_{22}(PPh_3)_2]^{2-}$, $[Pt_9(CO)_{16}(PPh_3)_2]^{2-}$, and $[Pt_6(CO)_{10}(PPh_3)_2]^{2-}$.

The reaction of $[Pt_9(CO)_{18}]^{2-}$ [ν(CO) 2029(s), 1839(m)] in acetone with 2 equiv of PPh_3 results in the immediate formation of the new species $[Pt_9(CO)_{16}(PPh_3)_2]^{2-}$ [ν(CO) 2016(s), 1824(m)] in accord with eq 1:

$$[Pt_9(CO)_{18}]^{2-} + 2PPh_3 \rightarrow [Pt_9(CO)_{16}(PPh_3)_2]^{2-} + 2CO \quad (1)$$

The substitution of two CO ligands with the more basic PPh_3 is confirmed by the lowering of the ν(CO) stretchings. Moreover, single crystals suitable for X-ray analyses of $[NBu_4]_2[Pt_9(CO)_{16}(PPh_3)_2]$ have been obtained by slow diffusion of n-hexane on the acetone solution. $[NBu_4]_2[Pt_9(CO)_{16}(PPh_3)_2]$ shows ν(CO) at 2021(vs), 2007(s), 1988(m), 1814(vs), and 1769(m) in nujol mull, and 2016(s), 1824(m) cm^{-1} in acetone. Its $^{31}P\{^1H\}$ NMR spectrum in deuterated acetone is displayed in Figure 2 together with the spectrum simulated using the program gNMR 5.0.6.0.[21] It must be remarked that the experimental spectrum at all temperatures displays the presence of a single species corresponding to $[Pt_9(CO)_{16}(PPh_3)_2]^{2-}$, indicating that no exchange process is present in solution.

The $^{31}P\{^1H\}$ NMR spectrum of $[Pt_9(CO)_{16}(PPh_3)_2]^{2-}$ fully agrees with its solid state structure (see Section 2.2). The two PPh_3 ligands are equivalent being terminally bonded to the two external Pt_3-triangles. Because of the isotopic distribution of Pt, they display a complex multiplet centered at δ_P 54.3 ppm with $^1J_{Pt-P}$ = 5144 Hz (to one Pt) and $^2J_{Pt-P}$ = 556 Hz (to two equivalent Pt-atoms). Each PPh_3 ligand is coupled to three Pt-atoms of the same triangle, whereas no coupling to the internal triangle is present. A similar situation has been previously found for the ^{13}C and ^{195}Pt NMR spectra of $[Pt_{3n}(CO)_{6n}]^{2-}$ (n = 2−6).[22] This is because the inter-triangular Pt−Pt bonds are considerably weaker than the intra-triangular ones.[9,10]

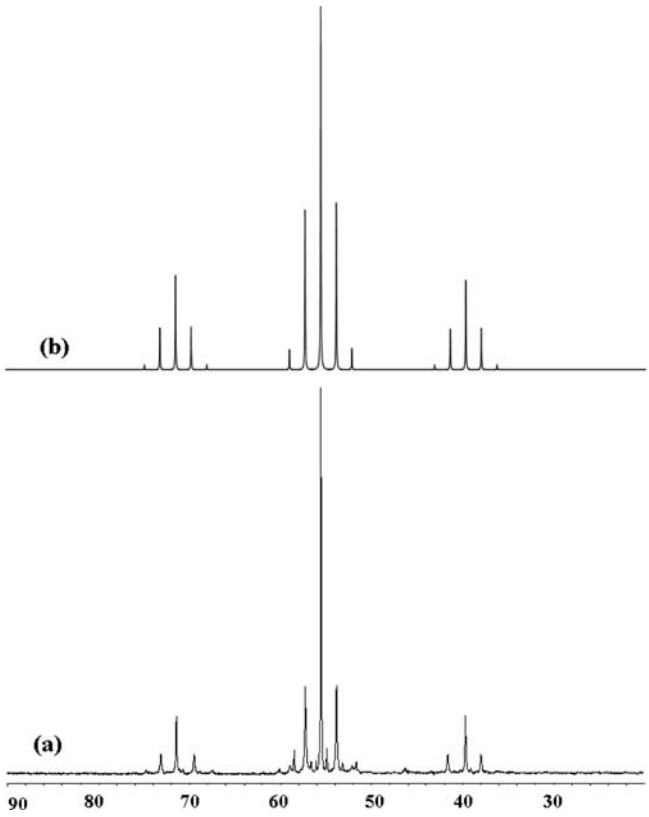

Figure 2. $^{31}P\{^1H\}$ NMR spectrum in deuterated acetone of pure $[Pt_9(CO)_{16}(PPh_3)_2]^{2-}$ at room temperature: (a) experimental and (b) simulated with gNMR 5.0.6.0.[21].

Similarly, $[Pt_{12}(CO)_{24}]^{2-}$ [ν(CO) 2047(s), 1868(m)] reacts with 2 equiv of PPh_3 affording the new $[Pt_{12}(CO)_{22}(PPh_3)_2]^{2-}$ anion [ν(CO) 2036(s), 1848(m) in acetone] in accord with eq 2:

$$[Pt_{12}(CO)_{24}]^{2-} + 2PPh_3 \rightarrow [Pt_{12}(CO)_{22}(PPh_3)_2]^{2-} + 2CO \quad (2)$$

As above, the ν(CO) stretchings are significantly lowered after substitution. X-ray quality crystals of $[NEt_4]_2[Pt_{12}(CO)_{22}(PPh_3)_2]$ have been obtained by slow diffusion of n-hexane on the acetone solution showing that

dx.doi.org/10.1021/ic3025414 | Inorg. Chem. 2013, 52, 4384−4395

also in this case the two PPh_3 ligands are bonded to the two external Pt_3-triangles (see Section 2.2). It must be noticed that the crystals of $[NEt_4]_2[Pt_{12}(CO)_{22}(PPh_3)_2]$ have been obtained in mixture with an amorphous powder containing $[Pt_9(CO)_{16}(PPh_3)_2]^{2-}$ and $[Pt_9(CO)_{17}(PPh_3)]^{2-}$ in a 1.5: 1: 1.1 ratio, as determined by $^{31}P\{^1H\}$ NMR spectroscopy. A few crystals have been mechanically separated from the amorphous solid for spectroscopic characterization.

$[NEt_4]_2[Pt_{12}(CO)_{22}(PPh_3)_2]$ displays ν(CO) at 2032(s), 2002(w), 1825(s), and 1780(s) in nujol mull, and 2036(s), 1848(m) cm^{-1} in acetone. Its $^{31}P\{^1H\}$ NMR spectrum in deuterated acetone is similar to the one of $[Pt_9(CO)_{16}(PPh_3)_2]^{2-}$ showing a multiplet at δ_P 50.6 ppm with $^1J_{Pt-P}$ = 5102 Hz (to one Pt) and $^2J_{Pt-P}$ = 551 Hz (to two equivalent Pt-atoms).

Conversely, $[Pt_6(CO)_{12}]^{2-}$ [ν(CO) 2001(s), 1800(m)] apparently does not react with PPh_3, since its IR spectrum remains unchanged. Nonetheless, $^{31}P\{^1H\}$ NMR spectroscopy indicates the formation of some new species containing PPh_3 bonded to Pt, and their concentration increases by increasing the amount of PPh_3. In particular, a few single crystals of $[NBu_4]_2[Pt_6(CO)_{10}(PPh_3)_2]$ have been obtained by slow diffusion of *n*-hexane on an acetone solution containing $[Pt_6(CO)_{12}]^{2-}$ and 10 equiv of PPh_3. Similarly, the solvate salt $[NBu_4]_2[Pt_6(CO)_{10}(PPh_3)_2]\cdot 2thf$ has been crystallized by slow diffusion of *n*-hexane on a thf solution containing $[Pt_6(CO)_{12}]^{2-}$ and 10 equiv of PPh_3. It must be remarked that in both cases the IR spectra showed the presence in solution of $[Pt_6(CO)_{12}]^{2-}$ as the major species. Moreover, only a few crystals of $[NBu_4]_2[Pt_6(CO)_{10}(PPh_3)_2]$ and $[NBu_4]_2[Pt_6(CO)_{10}(PPh_3)_2]\cdot 2thf$ have been obtained, whereas the majority of the solid was composed of amorphous $[Pt_6(CO)_{12}]^{2-}$ and traces of $[Pt_9(CO)_{16}(PPh_3)_2]^{2-}$, $[Pt_9(CO)_{15}(PPh_3)_3]^{2-}$, and $[Pt_6(CO)_{11}(PPh_3)]^{2-}$. This indicates that substitution of CO with PPh_3 is more difficult in the small $[Pt_6(CO)_{12}]^{2-}$ anion compared with higher nuclearity clusters having the same total charge. Thus, the reaction occurs only to a small extent, whereas the unsubstituted anion remains the predominant species (see Section 2.3 for further details).

The crystals of $[NBu_4]_2[Pt_6(CO)_{10}(PPh_3)_2]$ and $[NBu_4]_2[Pt_6(CO)_{10}(PPh_3)_2]\cdot 2thf$ display ν(CO) at 1973(s), 1960(vs), 1794(m) and 1756(vs) in nujol mull. It is noteworthy that such low frequencies bands are not observed in solution also after the addition of several equiv of PPh_3 to $[Pt_6(CO)_{12}]^{2-}$, confirming that this cluster is only present at low concentrations in the reaction mixtures. The $^{31}P\{^1H\}$ NMR spectrum of $[Pt_6(CO)_{10}(PPh_3)_2]^{2-}$ (in deuterated acetone) displays a pattern very similar to the ones reported for $[Pt_{12}(CO)_{22}(PPh_3)_2]^{2-}$ and $[Pt_9(CO)_{16}(PPh_3)_2]^{2-}$, displaying a multiplet centered at δ_P 56.5 ppm with $^1J_{Pt-P}$ = 5301 Hz (to one Pt) and $^2J_{Pt-P}$ = 566 Hz (to two equivalent Pt-atoms), in agreement with its solid state structure (see Section 2.2)

It is noteworthy that the ^{31}P chemical shifts for the three clusters $[Pt_{12}(CO)_{22}(PPh_3)_2]^{2-}$ (δ_P 50.6 ppm), $[Pt_9(CO)_{16}(PPh_3)_2]^{2-}$ (δ_P 54.3 ppm), and $[Pt_6(CO)_{10}(PPh_3)_2]^{2-}$ (δ_P 56.5 ppm) systematically move toward higher frequencies as the nuclearity decreases.

2.2. Crystal Structures of $[Pt_{12}(CO)_{22}(PPh_3)_2]^{2-}$, $[Pt_9(CO)_{16}(PPh_3)_2]^{2-}$, and $[Pt_6(CO)_{10}(PPh_3)_2]^{2-}$. The molecular structures of $[Pt_{12}(CO)_{22}(PPh_3)_2]^{2-}$, $[Pt_9(CO)_{16}(PPh_3)_2]^{2-}$, and $[Pt_6(CO)_{10}(PPh_3)_2]^{2-}$, as determined in their $[NEt_4]_2[Pt_{12}(CO)_{22}(PPh_3)_2]$, $[NBu_4]_2[Pt_9(CO)_{16}(PPh_3)_2]$, $[NBu_4]_2[Pt_6(CO)_{10}(PPh_3)_2]$ and $[NBu_4]_2[Pt_6(CO)_{10}(PPh_3)_2]\cdot 2thf$ salts, are represented in Figures 3–6, whereas their main bonding parameters are

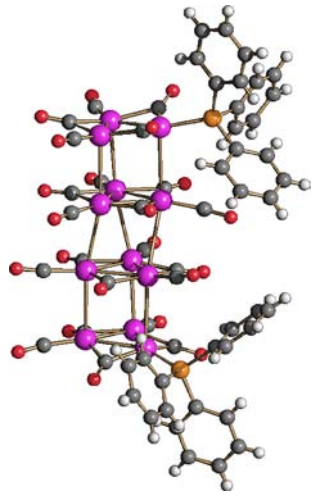

Figure 3. Molecular structure of $[Pt_{12}(CO)_{22}(PPh_3)_2]^{2-}$ (Pt, purple; P, orange; C, gray; O, red; H, white).

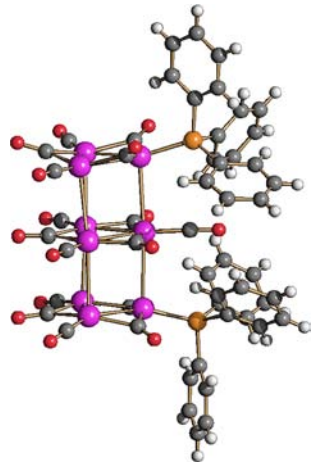

Figure 4. Molecular structure of $[Pt_9(CO)_{16}(PPh_3)_2]^{2-}$ (Pt, purple; P, orange; C, gray; O, red; H, white).

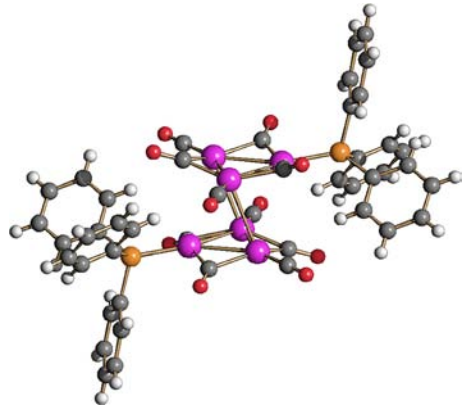

Figure 5. Molecular structure of $[Pt_6(CO)_{10}(PPh_3)_2]^{2-}$ as found in $[NBu_4]_2[Pt_6(CO)_{10}(PPh_3)_2]$ (Pt, purple; P, orange; C, gray; O, red; H, white).

dx.doi.org/10.1021/ic3025414 | *Inorg. Chem.* 2013, 52, 4384–4395

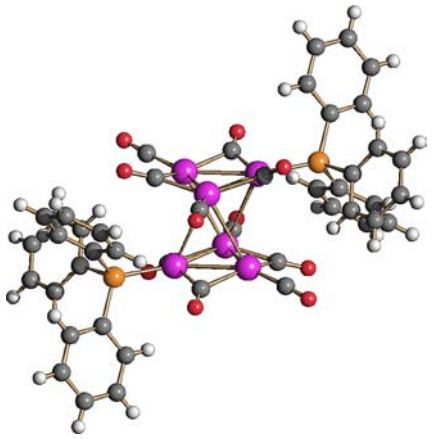

Figure 6. Molecular structure of $[Pt_6(CO)_{10}(PPh_3)_2]^{2-}$ as found in $[NBu_4]_2[Pt_6(CO)_{10}(PPh_3)_2]$·2thf (Pt, purple; P, orange; C, gray; O, red; H, white).

compared in Table 1 to those of the parent $[Pt_{12}(CO)_{24}]^{2-}$, $[Pt_9(CO)_{18}]^{2-}$, and $[Pt_6(CO)_{12}]^{2-}$.[9,10] The structure of the $[Pt_6(CO)_{10}(PPh_3)_2]^{2-}$ anion has been determined on two different solvate crystals, showing some interesting differences in the bonding parameters. In drawing Figures 3–6 it has been arbitrarily decided to represent Pt–Pt bonds up to 3.34 Å, which is slightly below twice the van der Waals radius of Pt and about 20% greater than twice its covalent radius (covalent radius 1.36 Å; van der Waals radius 1.72 Å).[23]

The molecular structures of both $[Pt_{12}(CO)_{22}(PPh_3)_2]^{2-}$ and $[Pt_9(CO)_{16}(PPh_3)_2]^{2-}$ are very similar to the parent $[Pt_{12}(CO)_{24}]^{2-}$ and $[Pt_9(CO)_{18}]^{2-}$ dianions,[9,10] the main difference being the replacement of two terminal CO with two PPh_3 ligands.

The inner $Pt_3(\mu\text{-}CO)_3(CO)_3$ triangular units (two and one, respectively) are coordinated to six CO ligands, three terminal and three edge bridging. Conversely, one terminal position of both external triangular units is occupied by a PPh_3 ligand. It is noteworthy that in $[Pt_{12}(CO)_{22}(PPh_3)_2]^{2-}$ and $[Pt_9(CO)_{16}(PPh_3)_2]^{2-}$ the two PPh_3 ligands are in a relative pseudo cis-position.

The intra-triangular Pt–Pt bonding distances of $[Pt_{12}(CO)_{22}(PPh_3)_2]^{2-}$ [2.6539(9)–2.6756(9) Å; average 2.666(2) Å] and $[Pt_9(CO)_{16}(PPh_3)_2]^{2-}$ [2.6597(8)–2.6814(9) Å; average 2.670(2) Å] compare very well to those found in the parent $[Pt_{12}(CO)_{24}]^{2-}$ [2.6587(5)–2.6707(5) Å; average 2.6656(12) Å] and $[Pt_9(CO)_{18}]^{2-}$ [2.65(2)–2.67(8) Å; average 2.66(9) Å] dianions,[9,10] for what concerns their ranges and average values. This suggests that the replacement of CO with PPh_3 does not alter the intra-triangular bonding contacts.

The inter-triangular contacts show similar average values in the PPh_3 substituted and unsubstituted clusters, but these values are more scattered in $[Pt_{12}(CO)_{22}(PPh_3)_2]^{2-}$ [3.0184(9)–3.2067(11) Å; average 3.086(2) Å] and $[Pt_9(CO)_{16}(PPh_3)_2]^{2-}$ [3.0015(9)–3.1098(8) Å; average 3.043(2) Å] compared to $[Pt_{12}(CO)_{24}]^{2-}$ [3.0465(5)–3.0597(5) Å; average 3.0535(12) Å] and $[Pt_9(CO)_{18}]^{2-}$ [3.04(2)–3.06(2) Å; average 3.05(4) Å]. This indicates that the substitution of CO with PPh_3 induces some local deformation of the inter-triangular bonding distances but, since some of them are elongated and others shortened, their average values do not change significantly compared to the parent unsubstituted dianions.

Conversely, the structure of $[Pt_6(CO)_{10}(PPh_3)_2]^{2-}$, as found in $[NBu_4]_2[Pt_6(CO)_{10}(PPh_3)_2]$ and $[NBu_4]_2[Pt_6(CO)_{10}(PPh_3)_2]$·2thf, significantly differs from $[Pt_{12}(CO)_{22}(PPh_3)_2]^{2-}$ and $[Pt_9(CO)_{16}(PPh_3)_2]^{2-}$, as well as the parent $[Pt_6(CO)_{12}]^{2-}$.[9]

$[Pt_6(CO)_{12}]^{2-}$ is a trigonal prism composed of two $Pt_3(\mu\text{-}CO)_3(CO)_3$ units with ideal D_{3h} symmetry (Figure 7a). Conversely, $[Pt_6(CO)_{10}(PPh_3)_2]^{2-}$, as found in both salts, is composed of two $Pt_3(\mu\text{-}CO)_3(CO)_2(PPh_3)$ units, which are rotated by 180° (taking the two PPh_3 ligands as references), ideally originating a trigonal antiprism which should include six inter-triangular Pt–Pt bonds. The structures of the $[Pt_6(CO)_{10}(PPh_3)_2]^{2-}$ anions depart from the ideal one, since only two inter-triangular Pt–Pt contacts [3.0353(6) Å] in the $[NBu_4]_2[Pt_6(CO)_{10}(PPh_3)_2]$ salt (Figure 7b) and four [3.1380(6) and 3.2079(6) Å, two by two equivalent] in $[NBu_4]_2[Pt_6(CO)_{10}(PPh_3)_2]$·2thf (Figure 7c) are at bonding distances, whereas the other ones [3.3581(6) and 3.5070(6) Å in $[NBu_4]_2[Pt_6(CO)_{10}(PPh_3)_2]$; 3.4310(6) Å in $[NBu_4]_2[Pt_6(CO)_{10}(PPh_3)_2]$·2thf] are basically nonbonding.

The fact that only $[Pt_6(CO)_{10}(PPh_3)_2]^{2-}$ shows a different geometry from the parent $[Pt_6(CO)_{12}]^{2-}$, whereas all higher nuclearity substituted and unsubstituted clusters are almost isostructural, is likely due to steric repulsion between the two bulky PPh_3 ligands in the smaller Pt_6 cluster. The slightly different structures found for $[Pt_6(CO)_{10}(PPh_3)_2]^{2-}$ in the two salts are due to different packing effects resulting from inclusion of thf in one salt. This points out that the inter-triangular bonds are rather weak and easily deformed by small changes in the van der Waals forces within the crystal.

2.3. Spectroscopic Investigation of the Reaction of $[Pt_{3n}(CO)_{6n}]^{2-}$ (n = 2–4) with PPh_3. The reactions described

Table 1. Main Bond Distances in $[Pt_{12}(CO)_{22}(PPh_3)_2]^{2-}$, $[Pt_9(CO)_{16}(PPh_3)_2]^{2-}$, and $[Pt_6(CO)_{10}(PPh_3)_2]^{2-}$, Compared to the Parent $[Pt_{12}(CO)_{24}]^{2-}$, $[Pt_9(CO)_{18}]^{2-}$, and $[Pt_6(CO)_{12}]^{2-}$

	Pt–Pt intra-triangular	Pt–Pt inter-triangular[a]	Pt–P
$[Pt_{12}(CO)_{22}(PPh_3)_2]^{2-}$	2.6539(9)–2.6756(9) average 2.666(2)	3.0184(9)–3.2067(11) average 3.086(2)	2.281(4)
$[Pt_{12}(CO)_{24}]^{2-}$[b]	2.6587(5)–2.6707(5) average 2.6656(12)	3.0465(5)–3.0597(5) average 3.0535(12)	
$[Pt_9(CO)_{16}(PPh_3)_2]^{2-}$	2.6597(8)–2.6814(9) average 2.670(2)	3.0015(9)–3.1098(8) average 3.043(2)	2.265(4)–2.287(4) average 2.276(6)
$[Pt_9(CO)_{18}]^{2-}$[b]	2.65(2)–2.67(8) average 2.66(9)	3.04(2)–3.06(2) average 3.05(4)	
$[Pt_6(CO)_{10}(PPh_3)_2]^{2-}$[c]	2.6558(6)–2.6743(6) average 2.6644(10)	3.0353(6)[e]	2.240(3)
$[Pt_6(CO)_{10}(PPh_3)_2]^{2-}$[d]	2.6584(6)–2.6787(6) average 2.6694(10)	3.1380(6)–3.2079(6) average 3.1729(8)[f]	2.247(3)
$[Pt_6(CO)_{12}]^{2-}$[b]	2.644(7)–2.659(3) average 2.653(10)	3.026(16)–3.049(17) average 3.03(3)	

[a]Only Pt–Pt interactions ≤3.34 Å have been included (see text). [b]From refs 9 and 10. [c]As found in $[NBu_4]_2[Pt_6(CO)_{10}(PPh_3)_2]$. [d]As found in $[NBu_4]_2[Pt_6(CO)_{10}(PPh_3)_2]$·2thf. [e]Three sets of inter-triangular Pt–Pt contacts are present: 3.0353(6), 3.3581(6), 3.5070(6) Å. [f]Three sets of inter-triangular Pt–Pt contacts are present: 3.1380(6), 3.2079(6), 3.4310(6) Å.

dx.doi.org/10.1021/ic3025414 | Inorg. Chem. 2013, 52, 4384–4395

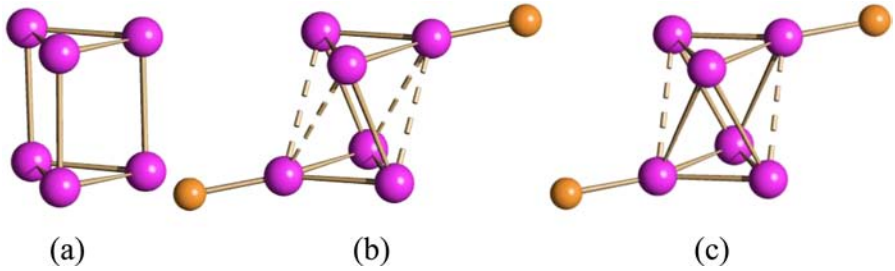

Figure 7. Metal frameworks of (a) $[Pt_6(CO)_{12}]^{2-}$, (b) $[Pt_6(CO)_{10}(PPh_3)_2]^{2-}$, as found in $[NBu_4]_2[Pt_6(CO)_{10}(PPh_3)_2]$ and (c) as found in $[NBu_4]_2[Pt_6(CO)_{10}(PPh_3)_2]\cdot 2thf$. (Pt, purple; P orange; Pt−Pt < 3.34 Å full line, Pt−Pt > 3.34 Å fragmented line).

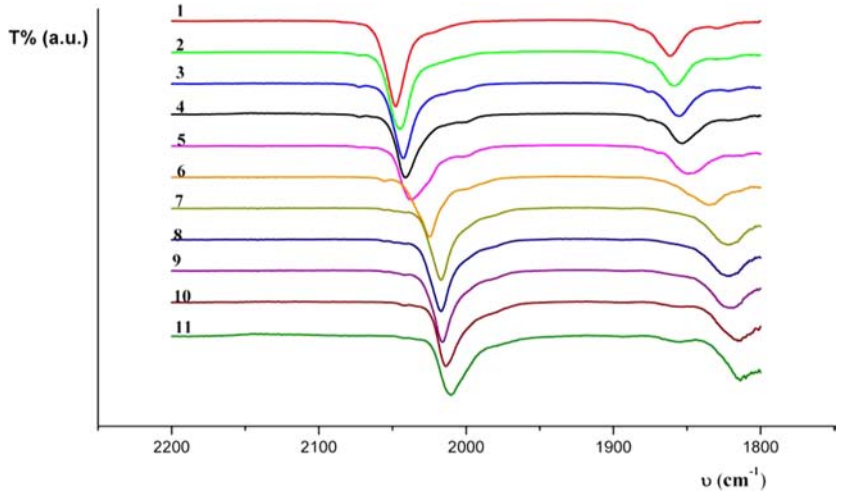

Figure 8. IR spectra in the ν(CO) region obtained by the stepwise addition of PPh_3 to an acetone solution of $[Pt_{12}(CO)_{24}]^{2-}$: (1) starting material; (2) +0.5 equiv.; (3) +1.0 equiv.; (4) +1.5 equiv.; (5) + 2.0 equiv.; (6) +3.0 equiv.; (7) +3.5 equiv.; (8) +4.5 equiv.; (9) +5.0 equiv.; (10) +6.5 equiv.; (11) +7.5 equiv.

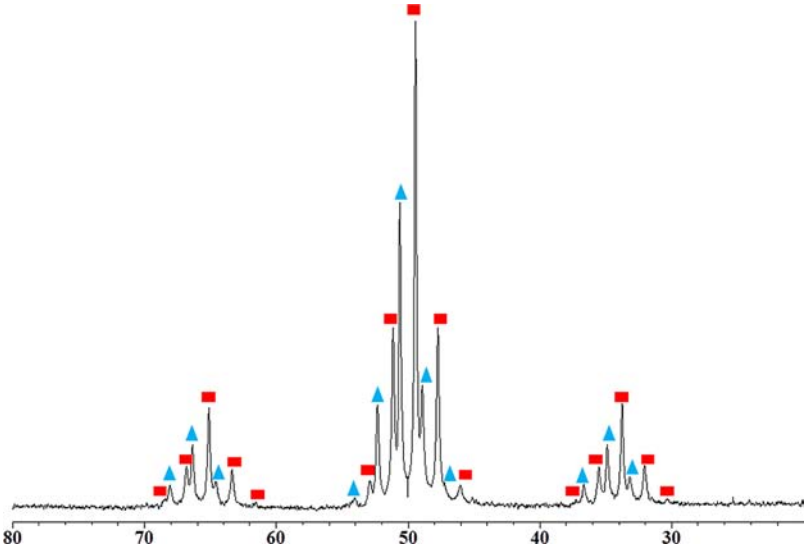

Figure 9. $^{31}P\{^1H\}$ NMR spectrum (in deuterated acetone) of $[Pt_{12}(CO)_{24}]^{2-}$ + 1 equiv of PPh_3. (red squares) $[Pt_{12}(CO)_{23}(PPh_3)]^{2-}$; (blue triangles) $[Pt_{12}(CO)_{22}(PPh_3)_2]^{2-}$.

in Section 2.1 show that it is possible to replace two CO ligands with PPh_3 in $[Pt_{3n}(CO)_{6n}]^{2-}$ (n = 2−4) without altering their metal cages. In this Section, we will spectroscopically investigate the possibility to substitute a different number of CO ligands.

The addition of small amounts of PPh_3 (0.5 equiv each time) to an acetone solution of $[Pt_{12}(CO)_{24}]^{2-}$ results in the gradual and continuous lowering of both terminal and bridging ν(CO) stretchings, as depicted in Figure 8.

After the addition of 1 equiv of PPh_3 to $[Pt_{12}(CO)_{24}]^{2-}$, the ν(CO) bands are lowered to 2042(s) and 1854(m) cm^{-1}, which is perfectly in the middle between the ν(CO) stretchings displayed by $[Pt_{12}(CO)_{24}]^{2-}$ and $[Pt_{12}(CO)_{22}(PPh_3)_2]^{2-}$. This

dx.doi.org/10.1021/ic3025414 | Inorg. Chem. 2013, 52, 4384−4395

apparently indicates the formation of the monosubstituted anion $[Pt_{12}(CO)_{23}(PPh_3)]^{2-}$ in agreement to eq 3:

$$[Pt_{12}(CO)_{24}]^{2-} + PPh_3 \rightarrow [Pt_{12}(CO)_{23}(PPh_3)]^{2-} + CO \quad (3)$$

To substantiate this conclusion, the same solution has been analyzed via $^{31}P\{^1H\}$ NMR spectroscopy (Figure 9).

The $^{31}P\{^1H\}$ NMR spectrum shows the presence of two main species in a 3:1 ratio. The minor product, which shows a multiplet centered at δ_P 50.6 ppm, is $[Pt_{12}(CO)_{22}(PPh_3)_2]^{2-}$ (see Section 2.1). The major species displays a similar pattern at δ_P 49.4 ppm with $^1J_{Pt-P}$ = 5081 Hz (to one Pt) and $^2J_{Pt-P}$ = 551 Hz (to two equivalent Pt-atoms), in agreement with the formation of $[Pt_{12}(CO)_{23}(PPh_3)]^{2-}$, in which the PPh_3 ligand is terminally bonded to a Pt_3 triangle. The ESI-MS spectrum of a CH_3CN solution containing $[Pt_{12}(CO)_{24}]^{2-}$ and 1 equiv of PPh_3 displays peaks at *m/z* (relative intensity in parentheses) 1506*(100)*, 1130*(10)*, 1625*(5)*, and 1883*(5)* attributable to $[Pt_{12}(CO)_{24}]^{2-}$, $[Pt_9(CO)_{18}]^{2-}$, $[Pt_{12}(CO)_{23}(PPh_3)]^{2-}$, and $[Pt_{15}(CO)_{30}]^{2-}$. The compositions of the solution determined by $^{31}P\{^1H\}$ NMR spectroscopy and ESI-MS are different, and this is probably due to the different sensitivity of these techniques and to the fact that some reactions may occur during ionization.[24] Therefore, the $^{31}P\{^1H\}$ NMR data are more reliable to determine the species present in solution, this technique being less invasive. Nonetheless, ESI-MS data confirm the formation of a monosubstituted $[Pt_{12}(CO)_{23}(PPh_3)]^{2-}$ species.

In addition, the spectroscopic data indicate that after the addition of 1 equiv of PPh_3 to $[Pt_{12}(CO)_{24}]^{2-}$ a mixture of products is present, and not a single species as it would have been expected on the basis of eq 3. Therefore, the first and second CO substitutions occur partially in parallel and not perfectly in sequence. This behavior also explains why the ν(CO) bands in Figure 8 are gradually and continuously lowered.

Similarly, the $^{31}P\{^1H\}$ NMR spectrum recorded after the addition of 2 equiv of PPh_3 to an acetone solution of $[Pt_{12}(CO)_{24}]^{2-}$ (Supporting Information, Figure S.1) shows the presence of a mixture of $[Pt_{12}(CO)_{22}(PPh_3)_2]^{2-}$, $[Pt_9(CO)_{16}(PPh_3)_2]^{2-}$, and $[Pt_9(CO)_{17}(PPh_3)]^{2-}$ in a 2.4: 1.6: 1 ratio. The presence in the same mixture of $[Pt_{12}(CO)_{24}]^{2-}$ and $[Pt_9(CO)_{18}]^{2-}$ cannot be ruled out nor confirmed by $^{31}P\{^1H\}$ NMR spectroscopy. These species have been detected in the ESI-MS spectrum of the same solution but, as explained above, it is not clear if they are formed during ionization or originally present in the solution.

The $^{31}P\{^1H\}$ NMR data for all the species studied in this paper are summarized in Table 2. Details on how all these data have been obtained are given in the Experimental Section, whereas spectra simulated with gNMR 5.0.6.0 are reported in the Supporting Information.[21] Simulations have been used to confirm the assignments, since the spectra are complicated because of the different isotopes of platinum.

The solutions containing $[Pt_{12}(CO)_{24}]^{2-}$, $[Pt_{12}(CO)_{23}(PPh_3)]^{2-}$, and $[Pt_{12}(CO)_{22}(PPh_3)_2]^{2-}$ as the major species display a typical green color. After the addition of 3 equiv of PPh_3 to $[Pt_{12}(CO)_{24}]^{2-}$ the solution turns from green to red, and the ν(CO) bands are shifted to 2024(s) and 1830(m) cm^{-1} significantly below the values reported for the red $[Pt_9(CO)_{18}]^{2-}$ anion [ν(CO) 2029(s), 1839(m) cm^{-1}].[9] $^{31}P\{^1H\}$ NMR spectroscopy shows the presence of a major species at δ_P 53.7 ppm with $^1J_{Pt-P}$ = 5022 Hz (to one Pt) and $^2J_{Pt-P}$ = 556 Hz (to two equivalent Pt-atoms), attributable to $[Pt_9(CO)_{17}(PPh_3)]^{2-}$. This assignment is based on the fact that this compound displays intermediate ν(CO) frequencies between $[Pt_9(CO)_{18}]^{2-}$ and $[Pt_9(CO)_{16}(PPh_3)_2]^{2-}$, as well as the same $^{31}P\{^1H\}$ NMR pattern of the latter shifted toward lower frequencies. Formation of $[Pt_9(CO)_{17}(PPh_3)]^{2-}$ starting from $[Pt_{12}(CO)_{24}]^{2-}$ may be described by eqs 4 and 5:

$$[Pt_{12}(CO)_{24}]^{2-} + 3PPh_3 \rightarrow [Pt_9(CO)_{18}]^{2-} + Pt_3(CO)_3(PPh_3)_3 + 3CO \quad (4)$$

$$[Pt_9(CO)_{18}]^{2-} + PPh_3 \rightarrow [Pt_9(CO)_{17}(PPh_3)]^{2-} + CO \quad (5)$$

Formation of $Pt_3(CO)_3(PPh_3)_3$ as side product was confirmed by IR and $^{31}P\{^1H\}$ NMR spectroscopy.[5] Moreover, the same compound $[Pt_9(CO)_{17}(PPh_3)]^{2-}$ may be obtained by the reaction of $[Pt_9(CO)_{18}]^{2-}$ with 1 equiv of PPh_3. The corresponding IR in acetone solution shows ν(CO) at 2024(s) and 1830(m) cm^{-1}, as above. The $^{31}P\{^1H\}$ NMR spectrum of a solution containing $[Pt_9(CO)_{18}]^{2-}$ and 1 equiv of PPh_3 shows that $[Pt_9(CO)_{17}(PPh_3)]^{2-}$ and $[Pt_9(CO)_{16}(PPh_3)_2]^{2-}$ are the major species present in a about 2: 1 ratio, together with some $[Pt_{12}(CO)_{23}(PPh_3)]^{2-}$ and $[Pt_{12}(CO)_{22}(PPh_3)_2]^{2-}$ (Supporting Information, Figure S.2).

The addition of 2 equiv of PPh_3 to $[Pt_9(CO)_{18}]^{2-}$ results in a further lowering of the ν(CO) bands at 2016(s) and 1824(m) cm^{-1}, in accord to the formation of $[Pt_9(CO)_{16}(PPh_3)_2]^{2-}$ (see Section 2.1). The $^{31}P\{^1H\}$ NMR spectrum of the crude solution (Supporting Information, Figure S.3) displays that a mixture of products is formed, containing $[Pt_9(CO)_{16}(PPh_3)_2]^{2-}$ and $[Pt_9(CO)_{15}(PPh_3)_3]^{2-}$ as the major species (ca. 2: 1 ratio) together with minor amounts of $[Pt_9(CO)_{17}(PPh_3)]^{2-}$ and $[Pt_{12}(CO)_{22}(PPh_3)_2]^{2-}$. As described in Section 2.1, crystals of $[NBu_4]_2[Pt_9(CO)_{16}(PPh_3)_2]$ have been obtained after layering *n*-hexane on this solution.

These results further confirm that the first and second CO substitution reactions occur partially in parallel. Moreover, a third CO may be replaced, affording $[Pt_9(CO)_{15}(PPh_3)_3]^{2-}$. Its $^{31}P\{^1H\}$ NMR spectrum shows two multiplets in a 2: 1 ratio centered at δ_P 57.3 and 55.0 ppm, respectively. The former displays $^1J_{Pt-P}$ = 5215 Hz (to one Pt atom), $^2J_{Pt-P}$ = 530 Hz (to two Pt-atoms), and $^3J_{P-P}$ = 50 Hz (to one P-atom), whereas the

Table 2. $^{31}P\{^1H\}$ NMR Data of $[Pt_{15}(CO)_{30-n}(PPh_3)_n]^{2-}$ (*n* = 1, 2), $[Pt_{12}(CO)_{24-n}(PPh_3)_n]^{2-}$ (*n* = 1, 2, 3), $[Pt_9(CO)_{18-n}(PPh_3)_n]^{2-}$ (*n* = 1, 2, 3), and $[Pt_6(CO)_{12-n}(PPh_3)_n]^{2-}$ (*n* = 1, 2) Recorded at Room Temperature in Deuterated Acetone

	δ_P (ppm)	$^1J_{Pt-P}$ (Hz)	$^2J_{Pt-P}$ (Hz)
$[Pt_{15}(CO)_{29}(PPh_3)]^{2-}$	47.0	5066	591
$[Pt_{15}(CO)_{28}(PPh_3)_2]^{2-}$	48.4	5065	569
$[Pt_{12}(CO)_{23}(PPh_3)]^{2-}$	49.4	5081	551
$[Pt_{12}(CO)_{22}(PPh_3)_2]^{2-}$	50.6	5102	551
$[Pt_9(CO)_{17}(PPh_3)]^{2-}$	53.7	5022	556
$[Pt_9(CO)_{16}(PPh_3)_2]^{2-}$	54.3	5144	556
$[Pt_9(CO)_{15}(PPh_3)_3]^{2-}$	55.0[a]	5338	549
	57.3[b]	5215	530
$[Pt_6(CO)_{11}(PPh_3)]^{2-}$	55.6	5222	540
$[Pt_6(CO)_{10}(PPh_3)_2]^{2-}$	56.5	5301	566

[a]Corresponding to a single P-atom. [b]Corresponding to two P-atoms. $^3J_{P-P}$ = 50 Hz.

dx.doi.org/10.1021/ic3025414 | *Inorg. Chem.* 2013, 52, 4384−4395

latter resonance displays the same pattern as the mono- and disubstituted clusters, with $^1J_{Pt-P}$ = 5338 Hz (to one Pt atom) and $^2J_{Pt-P}$ = 549 Hz (to two Pt-atoms). These data suggest that in the structure of $[Pt_9(CO)_{15}(PPh_3)_3]^{2-}$ two PPh_3 ligands are bonded to one external triangle and the third phosphine ligand to the other external Pt_3-triangle. P−P coupling is present between the two PPh_3 ligands on the same triangle, whereas no inter-triangular P−P nor P−Pt coupling has been detected. The possible isomer in which each Pt_3 triangle bears a single PPh_3 ligand can be ruled out on the basis of the observed $^{31}P\{^1H\}$ NMR pattern, whereas the isomer containing three PPh_3 ligands bonded to the same triangle would show a single resonance.

ESI-MS analysis of the same solution displays peaks at *m/z* (relative intensity in parentheses) 1481(*100*), 1247(*50*), 1365(*40*), 1740(*8*), and 1858(*4*) attributable to $[Pt_9(CO)_{15}(PPh_3)_3]^{2-}$, $[Pt_9(CO)_{17}(PPh_3)]^{2-}$, $[Pt_9(CO)_{16}(PPh_3)_2]^{2-}$, $[Pt_{12}(CO)_{22}(PPh_3)_2]^{2-}$, and $[Pt_{12}(CO)_{21}(PPh_3)_3]^{2-}$, respectively. Some minor peaks (intensity below 2%) are also present at *m/z* 870, 988, and 753 which may be assigned to $[Pt_6(CO)_{11}(PPh_3)]^{2-}$, $[Pt_6(CO)_{10}(PPh_3)_2]^{2-}$, and $[Pt_6(CO)_{12}]^{2-}$. As already discussed, the different compositions determined by $^{31}P\{^1H\}$ NMR spectroscopy and ESI-MS are mainly because reactions may occur during ionization. Nonetheless, ESI-MS data confirm the formation of a tris-substituted $[Pt_9(CO)_{15}(PPh_3)_3]^{2-}$ cluster, and suggest also the formation of an analogous higher nuclearity $[Pt_{12}(CO)_{21}(PPh_3)_3]^{2-}$ species.

Further addition of PPh_3 (three or more equiv) to $[Pt_9(CO)_{18}]^{2-}$ results in an orange solution displaying ν(CO) bands at 2001(s) and 1800(m) cm^{-1}, corresponding to $[Pt_6(CO)_{12}]^{2-}$.[9] Its formation is in accord with eq 6:

$$[Pt_9(CO)_{18}]^{2-} + 3PPh_3 \rightarrow [Pt_6(CO)_{12}]^{2-} + Pt_3(CO)_3(PPh_3)_3 + 3CO \quad (6)$$

The formation of $Pt_3(CO)_3(PPh_3)_3$ has been confirmed by means of IR and $^{31}P\{^1H\}$ NMR spectroscopy.[5]

Addition of PPh_3 to $[Pt_6(CO)_{12}]^{2-}$ does not result in any significant change in its ν(CO) bands and, only after the addition of a large excess of phosphine (>15 equiv), $[Pt_6(CO)_{12}]^{2-}$ is degraded to $Pt_3(CO)_3(PPh_3)_3$, $Pt(PPh_3)_2(CO)_2$, and $Pt(PPh_3)_3(CO)$, as indicated by IR and $^{31}P\{^1H\}$ NMR spectroscopy. The transformation of $Pt_3(CO)_3(PPh_3)_3$ into $Pt(PPh_3)_2(CO)_2$, $Pt(PPh_3)_3(CO)$, and other low nuclearity neutral Pt/CO/PPh_3 clusters after reaction with PPh_3 has been previously described in the literature.[5,6]

It is noteworthy that after the addition of 5 equiv of PPh_3 to $[Pt_6(CO)_{12}]^{2-}$ in acetone, the solution displays ν(CO) bands at 2001(s) and 1800(m) cm^{-1}, confirming that $[Pt_6(CO)_{12}]^{2-}$ is the major species present in solution. Nonetheless, the $^{31}P\{^1H\}$ NMR spectrum (Supporting Information, Figure S.4) reveals the presence also of $[Pt_6(CO)_{11}(PPh_3)]^{2-}$ and $[Pt_9(CO)_{16}(PPh_3)_2]^{2-}$ (ca. 5: 1 ratio) together with a minor amount of $[Pt_6(CO)_{10}(PPh_3)_2]^{2-}$. Moreover, crystals of $[Pt_6(CO)_{10}(PPh_3)_2]^{2-}$ have been obtained by slow diffusion of *n*-hexane on solutions containing $[Pt_6(CO)_{12}]^{2-}$ and 10 equiv of PPh_3 (see Section 2.1), even if IR spectroscopy indicated that $[Pt_6(CO)_{12}]^{2-}$ was the major species present in solution.

All the experiments described in Section 2.1 and 2.3 show that it is possible to replace 1−3 CO ligands in $[Pt_{3n}(CO)_{6n}]^{2-}$ with PPh_3. These substitution reactions afford complex mixtures of products. CO substitution in the smaller and more densely charged $[Pt_6(CO)_{12}]^{2-}$ is more difficult, in accord to the more basic character of PPh_3 compared to CO. Moreover, CO substitution competes with elimination of $Pt_3(CO)_3(PPh_3)_3$ and formation of lower nuclearity clusters.

2.4. Reaction of Higher Nuclearity $[Pt_{3n}(CO)_{6n}]^{2-}$ (*n* = 5,6) Clusters with PPh_3. In the case of higher nuclearity clusters such as $[Pt_{18}(CO)_{36}]^{2-}$ and $[Pt_{15}(CO)_{30}]^{2-}$, their reaction with PPh_3 mainly leads to $[Pt_{15}(CO)_{30}]^{2-}$ and $[Pt_{12}(CO)_{24}]^{2-}$, respectively, via inter-triangular Pt−Pt bond cleavage and elimination of $Pt_3(CO)_3(PPh_3)_3$. Also in these cases, the IR spectra recorded after addition of increasing amounts of PPh_3 show a gradual and continuous decrease of the ν(CO) frequencies (Supporting Information, Figure S.14) indicating that the CO ligands are partially substituted by PPh_3, but concomitant $^{31}P\{^1H\}$ NMR and ESI-MS analyses point out that unsubstituted $[Pt_{18}(CO)_{36}]^{2-}$, $[Pt_{15}(CO)_{30}]^{2-}$, and $[Pt_{12}(CO)_{24}]^{2-}$ are always the main species present in solution. At the moment, among the possible substitution products, there is direct evidence only for $[Pt_{15}(CO)_{29}(PPh_3)]^{2-}$ and $[Pt_{15}(CO)_{28}(PPh_3)_2]^{2-}$, which have been characterized by both ESI-MS and $^{31}P\{^1H\}$ NMR spectroscopy, whereas $[Pt_{18}(CO)_{35}(PPh_3)]^{2-}$ and $[Pt_{18}(CO)_{34}(PPh_3)_2]^{2-}$ have been detected only in traces (<0.5%) during ESI-MS studies. Therefore, we can conclude that these larger clusters promptly react with PPh_3 forming lower nuclearity species, making the isolation of the substituted clusters very difficult.

3. CONCLUSIONS

In the present paper, we have reported the first examples of anionic Pt/CO/PR_3 clusters, obtained by CO/PPh_3 substitution in $[Pt_{3n}(CO)_{6n}]^{2-}$ (*n* = 2−6) Chini's clusters. Three of them, that is, $[Pt_{12}(CO)_{22}(PPh_3)_2]^{2-}$, $[Pt_9(CO)_{16}(PPh_3)_2]^{2-}$, and $[Pt_6(CO)_{10}(PPh_3)_2]^{2-}$, have been structurally characterized showing a close analogy to $[Pt_{12}(CO)_{24}]^{2-}$ and $[Pt_9(CO)_{18}]^{2-}$ for the first two clusters, whereas, because of steric repulsion, the third one significantly differs from the parent $[Pt_6(CO)_{12}]^{2-}$. Two different structures of $[Pt_6(CO)_{10}(PPh_3)_2]^{2-}$ have been determined, showing that its metal cage can be easily deformed because of packing effects and van der Waals forces.

Moreover, combined IR, $^{31}P\{^1H\}$ NMR spectroscopy, and ESI-MS studies have revealed the presence in solution of several other substitution products, obtained by replacing 1−3 CO ligands with PPh_3 in $[Pt_{3n}(CO)_{6n}]^{2-}$ (*n* = 2−6). Substitution is, then, followed by elimination of $Pt_3(CO)_3(PPh_3)_3$ and formation of lower nuclearity clusters. These substitution/elimination reactions occur partially in parallel, leading to complex mixtures of products.

The reactions of metal carbonyl clusters with soft nucleophiles (e.g., CO, PR_3, RCCR, R_2CCR_2, pyridine, NO_2^-, halides) result either in the formation of addition or substitution products, or in cluster breakdown. The nature of the species formed depends on the nucleophile (which may or may not undergo transformation on the cluster surface), the type of metal cluster, and the conditions employed in the reaction. Generally, clusters of the lighter elements tend to fragment even under mild conditions, while those of the heavier elements, which are more robust, often afford addition and substitution products.[1,17−20] Unsaturated clusters may add ligands without any major structural rearrangement, whereas saturated clusters undergo CO substitution with retention of

dx.doi.org/10.1021/ic3025414 | *Inorg. Chem.* 2013, 52, 4384−4395

the structure, or ligand addition followed by metal−metal bond cleavage.[1,17−20,25] The latter may lead to the rearrangement of the cluster cage (e.g., from octahedral to trigonal prismatic) or to fragmentation and formation of lower nuclearity clusters. Ligands may also be activated and transformed after interaction with the cluster. It must be remarked that these studies have been mainly carried out on neutral clusters.

Conversely, the replacement of CO with PR_3 in anionic carbonyl clusters is not an obvious reaction, since the anionic charge should favor the presence of the more acidic CO compared to stronger σ-donors such as phosphines. At the moment, there is not in the literature any systematic study on the reactivity of high nuclearity anionic carbonyl clusters with phosphines and also the examples reported are scarce, compared to neutral clusters. We can expect that the reaction of an anionic carbonyl cluster with phosphines may lead to different results, such as CO substitution, cluster degradation, cluster condensation, or no reaction at all.

Most of the examples reported in the literature of CO substitution with PR_3 in anionic carbonyl clusters involve low nuclearity species, such as $[Fe_4N(CO)_{12}]^-$, $[Rh_6C(CO)_{15}]^{2-}$, $[Rh_6C(CO)_{13}]^{2-}$, and $[HIr_4(CO)_{11}]^-$. These react with PR_3 affording the isostructural $[Fe_4N(CO)_{11}(PR_3)]^-$,[26] $[Rh_6C(CO)_{14}(PPh_3)]^{2-}$,[27] $[Rh_6C(CO)_{11}(dppe)]^{2-}$,[28] and $[HIr_4(CO)_{10}(PPh_3)]^-$.[29] To the best of our knowledge, the largest anionic carbonyl cluster which undergoes direct CO substitution is $[HRu_{10}C(CO)_{24}]^-$, in which up to four carbonyls may be replaced by PR_3 ligands.[30]

More often, larger (and more charged) anionic carbonyl clusters do not react with phosphines or the reaction results in degradation to lower nuclearity species.[1,16] In some cases, this process has been used for the selective synthesis of homoleptic carbonyl clusters, such as the conversion of $[Ni_{13}Sb_2(CO)_{24}]^{3-}$ into $[Ni_{11}Sb_2(CO)_{18}]^{3-}$ by addition of PPh_3 and elimination of $Ni(CO)_3(PPh_3)$.[31] In a very few cases, an opposite process has been observed, that is, cluster condensation to higher nuclearity species upon treatment with PPh_3, such as for instance the formation of $[Ni_{16}(C_2)_2(CO)_{23}]^{2-}$ by reacting $[Ni_{10}C_2(CO)_{16}]^{2-}$ with PPh_3.[32]

Considering the data available in the literature, it seems that the substitution reaction is favored in anionic clusters possessing a robust metal cage. This is given, in the cases reported above, by the presence of interstitial heteroatoms or the involvement of heavier transition metals. In this respect, the $[Pt_{3n}(CO)_{6n}]^{2-}$ (n = 2−6) clusters herein studied are interesting since they are known to contain both strong intra-triangular Pt−Pt bonds and weaker inter-triangular ones.[9,10] The addition of stoichiometric amounts of PPh_3 initially results in CO replacement with retention of both intra- and inter-triangular Pt−Pt bonds. Then, further addition of phosphine results in the cleavage of the inter-triangular Pt−Pt bonds, elimination of $Pt_3(CO)_3(PPh_3)_3$, and formation of lower nuclearity anionic clusters, whereas the stronger intra-triangular Pt−Pt bonds remain intact. This clearly shows the competition between CO substitution and metal−metal bond cleavage in the reaction of anionic clusters with phosphines, as well as the possibility to control it by the stoichiometry of the reactions.

Finally, it must be remarked that the trigonal prismatic $[Pt_{3n}(CO)_{6n}]^{2-}$ (n = 2−6) Chini's clusters have been largely studied because of their chemical, structural, and self-assembly properties.[9,10,16] In addition, it has been recently reported that they are luminescent and behave as double emitting quantum dots.[33] These Pt clusters may be employed for homogeneous catalysis or as precursors of heterogeneous catalysts,[34−36] as well as printable metals in micro- and nanoelectronics.[15] The replacement of a few CO ligands with phosphines allows to modulate and tune the steric and electronic properties of these clusters and envisages the possibility of new applications. For instance, the clusters might be anchored on solid supports by using functionalized phosphines to prepare new polyfuntional materials with catalytic, electronic, or optical properties. Furthermore, tailored phosphines might be employed to couple such molecular clusters with metal nanoparticles or molecular compounds.

4. EXPERIMENTAL SECTION

4.1. General Procedures. All reactions and sample manipulations were carried out using standard Schlenk techniques under nitrogen and in dried solvents. All the reagents were commercial products (Aldrich) of the highest purity available and used as received, except $[NR_4]_2[Pt_{3n}(CO)_{6n}]$ (n = 2−6; R = Me, Bu)[9] which have been prepared according to the literature. Analyses of Pt were performed by atomic absorption on a Pye-Unicam instrument. Analyses of C, H, and N were obtained with a ThermoQuest FlashEA 1112NC instrument. IR spectra were recorded on a Perkin-Elmer SpectrumOne interferometer in CaF_2 cells. ESI mass spectra were recorded on a Waters Micromass ZQ4000 instrument. $^{31}P\{^1H\}$ NMR measurements were performed on a Varian Mercury Plus 400 MHz instrument. The phosphorus chemical shifts were referenced to external H_3PO_4 (85% in D_2O). $^{31}P\{^1H\}$ NMR spectra have been simulated with gNMR 5.0.6.0, using the experimental parameters (δ, J).[21] Structure drawings have been performed with SCHAKAL99.[37]

4.2. Synthesis of $[NEt_4]_2[Pt_{12}(CO)_{22}(PPh_3)_2]$. Solid PPh_3 (0.205 g, 0.782 mmol) was added in small portions to an acetone (20 mL) solution of $[NEt_4]_2[Pt_{12}(CO)_{24}]$ (1.28 g, 0.391 mmol). The solution was stirred at room temperature under nitrogen for 30 min. Then, the solvent was removed in vacuo, the solid washed with water (40 mL) and toluene (40 mL) and extracted in acetone (20 mL). Crystals of $[NEt_4]_2[Pt_{12}(CO)_{22}(PPh_3)_2]$ suitable for X-ray analyses were obtained by slow diffusion of n-hexane (40 mL). The crystals of $[NEt_4]_2[Pt_{12}(CO)_{22}(PPh_3)_2]$ were obtained in mixture with an amorphous powder containing $[Pt_9(CO)_{16}(PPh_3)_2]^{2-}$ and $[Pt_9(CO)_{17}(PPh_3)]^{2-}$ in a 1.5: 1: 1.1 ratio, as determined by $^{31}P\{^1H\}$ NMR. Therefore, it has not been possible to calculate the yield.

IR (acetone, 293 K) ν(CO): 2036(vs), 1848(m) cm^{-1}. IR (nujol mull, 293 K) ν(CO): 2032(s), 2002(w), 1825(s), 1780(s) cm^{-1}. $^{31}P\{^1H\}$ NMR (CD_3COCD_3, 298 K): δ_P 50.6 ppm, $^1J_{Pt-P}$ 5102 Hz, $^2J_{Pt-P}$ 551 Hz (Supporting Information, Figure S.10).

4.3. Synthesis of $[NBu_4]_2[Pt_9(CO)_{16}(PPh_3)_2]$. Solid PPh_3 (0.217 g, 0.830 mmol) was added in small portions to an acetone (20 mL) solution of $[NBu_4]_2[Pt_9(CO)_{18}]$ (1.14 g, 0.415 mmol). The solution was stirred at room temperature under nitrogen for 30 min. Then, the solvent was removed in vacuo, the solid washed with water (40 mL) and toluene (40 mL) and extracted in acetone (20 mL). Crystals of $[NBu_4]_2[Pt_9(CO)_{16}(PPh_3)_2]$ suitable for X-ray analyses were obtained by slow diffusion of n-hexane (40 mL) (yield 0.60 g, 45% based on Pt).

$C_{84}H_{102}N_2O_{16}P_2Pt_9$ (3213.43): calcd. C 31.39, H 3.20, N 0.87, Pt 54.64; found: C 31.52, H 3.02, N 0.71, Pt 54.89. IR (thf, 293 K) ν(CO): 2017(s), 1828(m) cm^{-1}. IR (acetone, 293 K) ν(CO): 2015(vs), 1823(m) cm^{-1}. IR (CH_3CN, 293 K) ν(CO): 2018(vs), 1820(m) cm^{-1}. IR (dmf, 293 K) ν(CO): 2014(vs), 1822(m) cm^{-1}. IR (nujol mull, 293 K) ν(CO): 2021(vs), 2007(s), 1988(m), 1814(vs), 1769(m) cm^{-1}. $^{31}P\{^1H\}$ NMR (CD_3COCD_3, 298 K): δ_P 54.3 ppm, $^1J_{Pt-P}$ 5144 Hz, $^2J_{Pt-P}$ 556 Hz (Supporting Information, Figure S.8).

4.4. Synthesis of $[NBu_4]_2[Pt_6(CO)_{10}(PPh_3)_2]$. Solid PPh_3 (1.50 g, 5.72 mmol) was added in small portions to an acetone (20 mL) solution of $[NBu_4]_2[Pt_6(CO)_{12}]$ (1.14 g, 0.572 mmol). The solution was stirred at room temperature under nitrogen for 30 min. Then, the solvent was removed in vacuo, the solid washed with water (40 mL) and toluene (40 mL) and extracted in acetone (20 mL). Crystals of

dx.doi.org/10.1021/ic3025414 | Inorg. Chem. 2013, 52, 4384−4395

$[NBu_4]_2[Pt_6(CO)_{10}(PPh_3)_2]$ suitable for X-ray analyses were obtained by slow diffusion of *n*-hexane (40 mL). Only a few crystals of $[NBu_4]_2[Pt_6(CO)_{10}(PPh_3)_2]$ were obtained, whereas the majority of the solid was composed of amorphous $[Pt_6(CO)_{12}]^{2-}$ with traces of $[Pt_9(CO)_{16}(PPh_3)_2]^{2-}$, $[Pt_9(CO)_{15}(PPh_3)_3]^{2-}$ and $[Pt_6(CO)_{11}(PPh_3)]^{2-}$. Therefore, it has not been possible to calculate the yield.

IR (nujol mull, 293 K) ν(CO): 1973(s), 1960(vs), 1794(m), 1756(vs) cm^{-1}. $^{31}P\{^1H\}$ NMR (CD_3COCD_3, 298 K): δ_P 56.5 ppm, $^1J_{Pt-P}$ 5301 Hz, $^2J_{Pt-P}$ 566 Hz (Supporting Information, Figure S.5).

4.5. Synthesis of $[NBu_4]_2[Pt_6(CO)_{10}(PPh_3)_2]\cdot 2thf$. Solid PPh_3 (1.50 g, 5.72 mmol) was added in small portions to an acetone (20 mL) solution of $[NBu_4]_2[Pt_6(CO)_{12}]$ (1.14 g, 0.572 mmol). The solution was stirred at room temperature under nitrogen for 30 min. Then, the solvent was removed in vacuo, the solid washed with water (40 mL) and toluene (40 mL) and extracted in thf (20 mL). Crystals of $[NBu_4]_2[Pt_6(CO)_{10}(PPh_3)_2]\cdot 2thf$ suitable for X-ray analyses were obtained by slow diffusion of *n*-hexane (40 mL). Only a few crystals of $[NBu_4]_2[Pt_6(CO)_{10}(PPh_3)_2]\cdot 2thf$ were obtained, whereas the majority of the solid was composed of amorphous $[Pt_6(CO)_{12}]^{2-}$ with traces of $[Pt_9(CO)_{16}(PPh_3)_2]^{2-}$, $[Pt_9(CO)_{15}(PPh_3)_3]^{2-}$, and $[Pt_6(CO)_{11}(PPh_3)]^{2-}$. Therefore, it has not been possible to calculate the yield.

IR (nujol mull, 293 K) ν(CO): 1973(s), 1960(vs), 1794(m), 1756(vs) cm^{-1}. $^{31}P\{^1H\}$ NMR (CD_3COCD_3, 298 K): δ_P 56.5 ppm, $^1J_{Pt-P}$ 5301 Hz, $^2J_{Pt-P}$ 566 Hz (Supporting Information, Figure S.5).

4.6. Stepwise Reaction of $[NBu_4]_2[Pt_{3n}(CO)_{6n}]$ (n = 2−6) with PPh_3. The stepwise reactions of $[NBu_4]_2[Pt_{3n}(CO)_{6n}]$ (n = 2−6) with PPh_3 were studied in acetone by adding increasing amounts of PPh_3 to an acetone solution of the cluster and monitoring the progress of the reaction via FT-IR. As an example, the experimental procedure for the reaction of $[NBu_4]_2[Pt_{12}(CO)_{24}]$ will be given.

Solid PPh_3 was added in small portions (45.4 mg each time, 0.173 mmol) to an acetone (20 mL) solution of $[NBu_4]_2[Pt_{12}(CO)_{24}]$ (1.21 g, 0.346 mmol). The solution was stirred at room temperature under nitrogen after each addition for 30 min and, then, its outcome checked via FT-IR in the same solvent. The different spectra recorded are reported in Figure 8.

The same procedure was employed for all the clusters of the $[NBu_4]_2[Pt_{3n}(CO)_{6n}]$ (n = 2−6) series affording analogous results, as described in Section 2.4. The cation employed does not influence the reaction.

4.7. ESI-MS and $^{31}P\{^1H\}$ NMR Studies on the Stepwise Reaction of $[NBu_4]_2[Pt_{3n}(CO)_{6n}]$ (n = 2−6) with PPh_3. These experiments were carried out exactly as described in Section 4.6, by adding the desired amount of PPh_3 to an acetone solution (20 mL) of $[NBu_4]_2[Pt_{3n}(CO)_{6n}]$ (n = 2−6) (ca. 0.35 mmol of cluster per experiment). The resulting solution was stirred at room temperature under nitrogen for 30 min and, then, the solvent removed under vacuo. The residue was washed with toluene (2 × 20 mL), and dried under vacuo. A small portion of the resulting solid was dissolved in CH_3CN for ESI-MS analyses, whereas the remaining part of the solid was dissolved in CD_3COCD_3 (0.8 mL) for the $^{31}P\{^1H\}$ NMR experiments. Some examples of the results obtained are described below. $^{31}P\{^1H\}$ NMR data are summarized in Table 2, whereas the spectra simulated with gNMR 5.0.6.0 are reported in the Supporting Information. Simulations have been performed using the experimental parameters (δ, J). The $^{31}P\{^1H\}$ NMR data for the compounds isolated as crystals have been directly determined on the pure species (Sections 4.2−4.5). For the other compounds, the $^{31}P\{^1H\}$ NMR data have been inferred from the analysis of several spectra obtained by mixing $[Pt_{3n}(CO)_6]^{2-}$ (n = 2−6) with different amounts of PPh_3, using the data of the crystalline compounds as references. Some of the experimental spectra used are given in the Supporting Information, Figures S1−S4. Since the $^{31}P\{^1H\}$ NMR spectra of these clusters are complicated by the presence of several isotopomers as well as mixtures of species, the assignments have been confirmed by comparing the experimental and simulated spectra.

(a). $[NBu_4]_2[Pt_{15}(CO)_{30}]$ + 1 equiv of PPh_3. IR (acetone, 293 K) ν(CO): 2056(s) and 1870(m) cm^{-1}.

$^{31}P\{^1H\}$ NMR (CD_3COCD_3, 293 K): the only species detected is $[Pt_{15}(CO)_{29}(PPh_3)]^{2-}$ (its data are summarized in Table 2).

ESI-MS (CH_3CN): ES- m/z (relative intensity in parentheses): 1507(*100*), 1883(*70*), 2002(*15*), 2261(*18*), and 1623(*5*) attributable to $[Pt_{12}(CO)_{24}]^{2-}$, $[Pt_{15}(CO)_{30}]^{2-}$, $[Pt_{15}(CO)_{29}(PPh_3)]^{2-}$, $[Pt_{18}(CO)_{36}]^{2-}$, and $[Pt_{12}(CO)_{23}(PPh_3)]^{2-}$, respectively. Some minor peaks (intensity below 1%) are also present at m/z 2118, 2379, and 2497 which may be assigned to $[Pt_{15}(CO)_{28}(PPh_3)_2]^{2-}$, $[Pt_{18}(CO)_{35}(PPh_3)]^{2-}$, and $[Pt_{18}(CO)_{34}(PPh_3)_2]^{2-}$.

(b). $[NBu_4]_2[Pt_{15}(CO)_{30}]$ + 1.5 equiv of PPh_3. IR (acetone, 293 K) ν(CO): 2054(s) and 1867(m) cm^{-1}.

$^{31}P\{^1H\}$ NMR (CD_3COCD_3, 293 K): no species detected, a part of a very weak resonance probably attributable to $[Pt_{15}(CO)_{29}(PPh_3)]^{2-}$ (its data are summarized in Table 2).

ESI-MS (CH_3CN): ES- m/z (relative intensity in parentheses): 1884(*100*), 1506(*98*), 2260(*20*), and 2000(*2*) attributable to $[Pt_{15}(CO)_{30}]^{2-}$, $[Pt_{12}(CO)_{24}]^{2-}$, $[Pt_{18}(CO)_{36}]^{2-}$, and $[Pt_{15}(CO)_{29}(PPh_3)]^{2-}$, respectively. Some minor peaks (intensity below 1%) are also present at m/z 2118, 2379, and 2497 which may be assigned to $[Pt_{15}(CO)_{28}(PPh_3)_2]^{2-}$, $[Pt_{18}(CO)_{35}(PPh_3)]^{2-}$, and $[Pt_{18}(CO)_{34}(PPh_3)_2]^{2-}$.

(c). $[NBu_4]_2[Pt_{12}(CO)_{24}]$ + 1 equiv of PPh_3. IR (acetone, 293 K) ν(CO): 2042(s) and 1854(m) cm^{-1}.

$^{31}P\{^1H\}$ NMR (CD_3COCD_3, 293 K): species detected $[Pt_{12}(CO)_{23}(PPh_3)]^{2-}$ and $[Pt_{12}(CO)_{22}(PPh_3)_2]^{2-}$ as the major species (ca. 3: 1 ratio) together with minor amount of $[Pt_9(CO)_{17}(PPh_3)]^{2-}$ (their data are summarized in Table 2; for the experimental spectrum see Figure 9).

ESI-MS (CH_3CN): ES- m/z (relative intensity in parentheses): 1506*(100)*, 1130*(10)*, 1625*(5)*, and 1883*(5)* attributable to $[Pt_{12}(CO)_{24}]^{2-}$, $[Pt_9(CO)_{18}]^{2-}$, $[Pt_{12}(CO)_{23}(PPh_3)]^{2-}$, $[Pt_{15}(CO)_{30}]^{2-}$.

(d). $[NBu_4]_2[Pt_9(CO)_{18}]$ + 1 equiv of PPh_3. IR (acetone, 293 K) ν(CO): 2024(s) and 1830(m) cm^{-1}.

$^{31}P\{^1H\}$ NMR (CD_3COCD_3, 293 K): species detected $[Pt_9(CO)_{17}(PPh_3)]^{2-}$ and $[Pt_9(CO)_{16}(PPh_3)_2]^{2-}$ as the major species in a about 2: 1 ratio, together with minor amounts of $[Pt_{12}(CO)_{23}(PPh_3)]^{2-}$ and $[Pt_{12}(CO)_{22}(PPh_3)_2]^{2-}$ (their data are summarized in Table 2; for the experimental spectrum see Supporting Information, Figure S.2).

ESI-MS (CH_3CN): ES- m/z (relative intensity in parentheses): 1247(*100*), 1130(*45*), 1365(*35*), 1741(*30*), and 1623(*20*) attributable to $[Pt_9(CO)_{17}(PPh_3)]^{2-}$, $[Pt_9(CO)_{18}]^{2-}$, $[Pt_9(CO)_{16}(PPh_3)_2]^{2-}$, $[Pt_{12}(CO)_{22}(PPh_3)_2]^{2-}$, and $[Pt_{12}(CO)_{23}(PPh_3)]^{2-}$, respectively. Some minor peaks (intensity below 2%) are also present at m/z 1859 and 1804 which may be assigned to $[Pt_{12}(CO)_{21}(PPh_3)_3]^{2-}$ and $[Pt_{12}(CO)_{24}]^{2-}$.

(e). $[NBu_4]_2[Pt_9(CO)_{18}]$ + 2 equiv of PPh_3. IR (acetone, 293 K) ν(CO): 2016(s) and 1824(m) cm^{-1}.

$^{31}P\{^1H\}$ NMR (CD_3COCD_3, 293 K): species detected $[Pt_9(CO)_{16}(PPh_3)_2]^{2-}$ and $[Pt_9(CO)_{15}(PPh_3)_3]^{2-}$ as the major species (ca. 2: 1 ratio) together with minor amounts of $[Pt_9(CO)_{17}(PPh_3)]^{2-}$ and $[Pt_{12}(CO)_{22}(PPh_3)_2]^{2-}$ (their data are summarized in Table 2; for the experimental spectrum see Supporting Information, Figure S.3).

ESI-MS (CH_3CN): ES- m/z (relative intensity in parentheses): 1481(*100*), 1247(*50*), 1365(*40*), 1740(*8*), and 1858*(4)* attributable to $[Pt_9(CO)_{15}(Ph_3)_3]^{2-}$, $[Pt_9(CO)_{17}(PPh_3)]^{2-}$, $[Pt_9(CO)_{16}(PPh_3)_2]^{2-}$, $[Pt_{12}(CO)_{22}(PPh_3)_2]^{2-}$, and $[Pt_{12}(CO)_{21}(PPh_3)_3]^{2-}$, respectively. Some minor peaks (intensity below 2%) are also present at m/z 870, 988, and 753 which may be assigned to $[Pt_6(CO)_{11}(PPh_3)]^{2-}$, $[Pt_6(CO)_{10}(PPh_3)_2]^{2-}$, and $[Pt_6(CO)_{12}]^{2-}$.

(f). $[NBu_4]_2[Pt_6(CO)_{12}]$ + 5 equiv of PPh_3. IR (acetone, 293 K) ν(CO): 2002(s) and 1823(w) cm^{-1} attributable to $[Pt_6(CO)_{12}]^{2-}$.

$^{31}P\{^1H\}$ NMR (CD_3COCD_3, 293 K): species detected $[Pt_6(CO)_{11}(PPh_3)]^{2-}$ and $[Pt_9(CO)_{16}(PPh_3)_2]^{2-}$ as the major species (ca. 5: 1 ratio) together with a minor amount of $[Pt_6(CO)_{10}(PPh_3)_2]^{2-}$ (their data are summarized in Table 2; for the experimental spectrum see Supporting Information, Figure S.4).

ESI-MS (CH_3CN): the sample is likely to be oxidized during the analysis as demonstrated by the presence of larger clusters in the mass

dx.doi.org/10.1021/ic3025414 | *Inorg. Chem.* 2013, 52, 4384−4395

Table 3. Crystal Data and Experimental Details for $[NBu_4]_2[Pt_6(CO)_{10}(PPh_3)_2]$, $[NBu_4]_2[Pt_6(CO)_{10}(PPh_3)_2]\cdot 2thf$, $[NBu_4]_2[Pt_9(CO)_{16}(PPh_3)_2]$, and $[NEt_4]_2[Pt_{12}(CO)_{22}(PPh_3)_2]$

	$[NBu_4]_2[Pt_6(CO)_{10}(PPh_3)_2]$	$[NBu_4]_2[Pt_6(CO)_{10}(PPh_3)_2]\cdot 2thf$	$[NBu_4]_2[Pt_9(CO)_{16}(PPh_3)_2]$	$[NEt_4]_2[Pt_{12}(CO)_{22}(PPh_3)_2]$
formula	$C_{78}H_{102}N_2O_{10}P_2Pt_6$	$C_{86}H_{118}N_2O_{12}P_2Pt_6$	$C_{84}H_{102}N_2O_{16}P_2Pt_9$	$C_{74}H_{70}N_2O_{22}P_2Pt_{12}$
Fw	2460.10	2604.30	3213.43	3742.34
T, K	295(2)	100(2)	100(2)	295(2)
λ, Å	0.71073	0.71073	0.71073	0.71073
crystal system	monoclinic	monoclinic	monoclinic	monoclinic
space group	$P2_1/n$	$P2_1/n$	$P2_1/n$	$C2/c$
a, Å	12.1277(12)	17.3714(9)	15.2430(10)	15.5382(13)
b, Å	23.282(2)	13.3264(7)	24.5212(16)	20.7765(17)
c, Å	14.4729(14)	19.5839(10)	24.5500(16)	27.887(3)
β, deg	91.3210(10)	108.1410(10)	102.7780(10)	105.5300(10)
cell volume, Å^3	4085.4(7)	4308.3/4)	8949.0(10)	8674.2(13)
Z	2	2	4	4
D_c, g cm^{-3}	2.000	2.008	2.385	2.866
μ, mm^{-1}	10.327	9.800	14.107	19.371
F(000)	2324	2484	5920	6680
crystal size, mm	0.16 × 0.15 × 0.10	0.16 × 0.15 × 0.10	0.15 × 0.12 × 0.11	0.16 × 0.14 × 0.10
θ limits, deg	1.66−26.00	1.37−26.00	1.44−25.03	1.52−25.03
index ranges	$-14 \le h \le 14$	$-20 \le h \le 21$	$-18 \le h \le 18$	$-18 \le h \le 18$
	$-28 \le k \le 28$	$-16 \le k \le 16$	$-29 \le k \le 29$	$-24 \le k \le 24$
	$-17 \le l \le 17$	$-24 \le l \le 24$	$-29 \le l \le 29$	$-33 \le l \le 33$
reflections collected	419555	39055	84627	41538
independent reflections	8007 [R_{int} = 0.0954]	8463 [R_{int} = 0.1182]	15812 [R_{int} = 0.0915]	7665 [R_{int} = 0.0843]
completeness to *θ* max	99.9	99.9	99.9%	99.8
data/restraints/parameters	8007/438/479	8463/224/462	15812/589/1018	7665/318/498
goodness on fit on F^2	1.003	1.003	1.009	0.996
R_1 ($I > 2\sigma(I)$)	0.0406	0.0436	0.0486	0.0444
wR_2 (all data)	0.0820	0.0908	0.1261	0.1072
largest diff. peak and hole, e Å^{-3}	0.723/−0.576	1.686/−1.292	1.790/−1.487	1.296/−0.981

spectrum. ES- *m*/*z* (relative intensity in parentheses): 1246(*100*), 1365(*95*), and 871(*20*) attributable to $[Pt_9(CO)_{17}(PPh_3)]^{2-}$, $[Pt_9(CO)_{16}(PPh_3)_2]^{2-}$, and $[Pt_6(CO)_{11}(PPh_3)]^{2-}$, respectively.

4.8. X-ray Crystallographic Study. Crystal data and collection details for $[NBu_4]_2[Pt_6(CO)_{10}(PPh_3)_2]$, $[NBu_4]_2[Pt_6(CO)_{10}(PPh_3)_2]\cdot 2thf$, $[NBu_4]_2[Pt_9(CO)_{16}(PPh_3)_2]$, and $[NEt_4]_2[Pt_{12}(CO)_{22}(PPh_3)_2]$ are reported in Table 3. The diffraction experiments were carried out on a Bruker APEX II diffractometer equipped with a CCD detector using Mo−K*α* radiation. Data were corrected for Lorentz polarization and absorption effects (empirical absorption correction SADABS).[38] Structures were solved by direct methods and refined by full-matrix least-squares based on all data using F^2.[39] Hydrogen atoms were fixed at calculated positions and refined by a riding model. All non-hydrogen atoms were refined with anisotropic displacement parameters.

$[NBu_4]_2[Pt_6(CO)_{10}(PPh_3)_2]$. The asymmetric unit of the unit cell contains half of a cluster anion (on an inversion center) and one $[NBu_4]^+$ cation (on general position). Similar *U* restraints (s.u. 0.01) were applied to the C and O atoms. Restraints to bond distances were applied as follow (s.u. 0.01): 1.53 Å for C−C and 1.47 Å for C−N in $[NBu_4]^+$. One n-Bu group of $[NBu_4]^+$ is disordered over two positions: disordered atomic positions were split and refined anisotropically using similar geometries (SAME line in SHELXL; s.u. 0.02) and similar *U* (SIMU line in SHELXL; s.u. 0.01) restraints and one occupancy parameter per disordered group.

$[NBu_4]_2[Pt_6(CO)_{10}(PPh_3)_2]\cdot 2thf$. The asymmetric unit of the unit cell contains half of a cluster anion (on an inversion center), one $[NBu_4]^+$ cation (on general position), and one thf molecule (on general position). Similar *U* restraints (s.u. 0.01) were applied to the C and O atoms. The thf molecule was treated isotropically. Restraints to bond distances were applied as follow (s.u. 0.01): 1.53 Å for C−C and 1.43 Å for C−O in thf.

$[NBu_4]_2[Pt_9(CO)_{16}(PPh_3)_2]$. The asymmetric unit of the unit cell contains one cluster anion and two $[NBu_4]^+$ cations (all located on general positions). Similar *U* restraints (s.u. 0.005) were applied to the C and O atoms. Restraints to bond distances were applied as follow (s.u. 0.01): 1.53 Å for C−C and 1.47 Å for C−N in $[NBu_4]^+$. The geometries of the $[NBu_4]^+$ cations were restrained to be similar (SAME line in SHELXL; s.u. 0.02).

$[NEt_4]_2[Pt_{12}(CO)_{22}(PPh_3)_2]$. The asymmetric unit of the unit cell contains half of a cluster anion (on a 2-fold axis) and one $[NEt_4]^+$ cation (on general position). Similar *U* restraints (s.u. 0.005) were applied to the C and O atoms. Restraints to bond distances were applied as follow (s.u. 0.01): 1.53 Å for C−C and 1.47 Å for C−N in $[NEt_4]^+$. The $[NEt_4]^+$ cation is disordered over two positions: disordered atomic positions were split and refined isotropically using similar geometries (SAME line in SHELXL; s.u. 0.02) and similar *U* (SIMU line in SHELXL; s.u. 0.01) restraints and one occupancy parameter per disordered group.

■ ASSOCIATED CONTENT

Supporting Information

CIF files giving X-ray crystallographic data for the structure determination of $[NBu_4]_2[Pt_6(CO)_{10}(PPh_3)_2]$, $[NBu_4]_2[Pt_6(CO)_{10}(PPh_3)_2]\cdot 2thf$, $[NBu_4]_2[Pt_9(CO)_{16}(PPh_3)_2]$, and $[NEt_4]_2[Pt_{12}(CO)_{22}(PPh_3)_2]$. Some representative experimental $^{31}P\{^1H\}$ NMR spectra of the compounds described in the text and their $^{31}P\{^1H\}$ NMR spectra simulated with gNMR 5.0.6.0. IR spectra in the *ν*(CO) region obtained by the stepwise addition of PPh_3 to an acetone solution of $[Pt_{18}(CO)_{36}]^{2-}$. This material is available free of charge via the Internet at http://pubs.acs.org.

dx.doi.org/10.1021/ic3025414 | *Inorg. Chem.* 2013, 52, 4384−4395

AUTHOR INFORMATION

Corresponding Author

*Fax: +39 0512093690. E-mail: stefano.zacchini@unibo.it.

Notes

The authors declare no competing financial interest.

ACKNOWLEDGMENTS

The financial support of MIUR (PRIN2008) and the University of Bologna is gratefully acknowledged. Funding by Fondazione CARIPLO, Project No. 2011-0289, is heartily acknowledged. We thank the Reviewers for the very useful suggestions in revising the manuscript.

REFERENCES

(1) (a) Schmid, G., Ed.; *Clusters and Colloids*; Wiley-VCH: New York, 1994. (b) Braunstein, P.; Oro, L. A.; Raithby, P. R., Eds.; *Metal Clusters in Chemistry*; Wiley-VCH: New York, 1999.

(2) Mednikov, E. G.; Dahl, L. F. *Phil Trans. R. Soc. A* **2010**, *368*, 1301.

(3) (a) Kawano, M.; Bacon, J. W.; Campana, C. F.; Dahl, L. F. *J. Am. Chem. Soc.* **1996**, *118*, 7869. (b) Kawano, M.; Bacon, J. W.; Campana, C. F.; Winger, B. E.; Dudek, J. D.; Sirchio, S. A.; Scruggs, S. A.; Geiser, U.; Dahl, L. F. *Inorg. Chem.* **2001**, *40*, 2554.

(4) (a) Tran, N. T.; Powell, D. R.; Dahl, L. F. *Dalton Trans.* **2004**, 209. (b) Kawano, M.; Bacon, J. W.; Campana, C. F.; Dahl, L. F. *J. Am. Chem. Soc.* **1996**, *118*, 7869. (c) Willocq, C.; Tinant, B.; Aubriet, F.; Carré, V.; Devillers, M. *Inorg. Chim. Acta* **2011**, *373*, 233.

(5) (a) Booth, G.; Chatt, J.; Chini, P. *Chem. Commun.* **1965**, 639. (b) Chatt, J.; Chini, P. *J. Chem. Soc. A* **1970**, 1538. (c) Béni, Z.; Ros, R.; Tassan, A.; Scopelliti, R.; Roulet, R. *Inorg. Chim. Acta* **2005**, *358*, 497.

(6) (a) Ivanov, S. A.; de Silva, N.; Kozee, M. A.; Nichiporuk, R. V.; Dahl, L. F. *J. Cluster Sci.* **2004**, *15*, 233. (b) Howard, J. A. K.; Spencer, J. L.; Turner, D. G. *J. Chem. Soc., Dalton Trans.* **1987**, 259.

(7) (a) Kurasov, S. S.; Eremenko, N. K.; Slovokhotov, Yu. L.; Struchkov, Yu. T *J. Organomet. Chem.* **1989**, *361*, 405. (b) de Silva, N.; Dahl, L. F. *Inorg. Chem.* **2005**, *44*, 9604.

(8) (a) Ferguson, G.; Lloyd, B. R.; Puddephatt, R. J. *Organometallics* **1986**, *5*, 344. (b) Hao, L.; Spivak, G. J.; Xiao, J.; Vittal, J. J.; Puddephatt, R. J. *J. Am. Chem. Soc.* **1995**, *117*, 7011.

(9) (a) Longoni, G.; Chini, P. *J. Am. Chem. Soc.* **1976**, *98*, 7225. (b) Calabrese, J. C.; Dahl, L. F.; Chini, P.; Longoni, G.; Martinengo, S. *J. Am. Chem. Soc.* **1974**, *96*, 2614.

(10) (a) Femoni, C.; Kaswalder, F.; Iapalucci, M. C.; Longoni, G.; Mehlstäubl, M.; Zacchini, S. *Chem. Commun.* **2005**, *46*, 5769. (b) Femoni, C.; Kaswalder, F.; Iapalucci, M. C.; Longoni, G.; Mehlstäubl, M.; Zacchini, S.; Ceriotti, A. *Angew. Chem., Int. Ed.* **2006**, *45*, 2060. (c) Femoni, C.; Kaswalder, F.; Iapalucci, M. C.; Longoni, G.; Zacchini, S. *Eur. J. Inorg. Chem.* **2007**, 1483. (d) Femoni, C.; Iapalucci, M. C.; Longoni, G.; Lovato, T.; Stagni, S.; Zacchini, S. *Inorg. Chem.* **2010**, *49*, 5992.

(11) Gao, F.; Li, C.; Heaton, B. T.; Zacchini, S.; Zarra, S.; Longoni, G.; Garland, M. *Dalton Trans.* **2011**, *40*, 5002.

(12) (a) Washecheck, D. M.; Wucherer, E. J.; Dahl, L. F.; Ceriotti, A.; Longoni, G.; Manassero, M.; Sansoni, M.; Chini, P. *J. Am. Chem. Soc.* **1979**, *101*, 6110. (b) Ceriotti, A.; Masciocchi, N.; Macchi, P.; Longoni, G. *Angew. Chem., Int. Ed.* **1999**, *38*, 3724. (c) Fedi, S.; Zanello, P.; Laschi, F.; Ceriotti, A.; El Afefey, S. *J. Solid State Electrochem.* **2009**, *13*, 1497.

(13) Roth, J. D.; Lewis, G. J.; Safford, L. K.; Jiang, X.; Dahl, L. F.; Weaver, M. J. *J. Am. Chem. Soc.* **1992**, *114*, 6159.

(14) (a) Chini, P. *J. Organomet. Chem.* **1980**, *200*, 37. (b) Ceriotti, A.; Masciocchi, N.; Macchi, P.; Longoni, G. *Angew. Chem., Int. Ed.* **1999**, *38*, 3724.

(15) (a) Greco, P.; Cavallini, M.; Stoliar, P.; Quiroga, S. D.; Dutta, S.; Zacchini, S.; Iapalucci, M. C.; Morandi, V.; Milita, S.; Merli, P. G.; Biscarini, F. *J. Am. Chem. Soc.* **2008**, *130*, 1177. (b) Serban, D. A.; Greco, P.; Melinte, S.; Vlad, A.; Dutu, C. A.; Zacchini, S.; Iapalucci, M. C.; Biscarini, F.; Cavallini, M. *Small* **2009**, *5*, 1117.

(16) (a) Femoni, C.; Kaswalder, F.; Iapalucci, M. C.; Longoni, G.; Zacchini, S. *Coord. Chem. Rev.* **2006**, *250*, 1580. (b) Zacchini, S. *Eur. J. Inorg. Chem.* **2011**, 4125.

(17) Vargas, M. D.; Nicholls, J. N. *Adv. Inorg. Chem. Radiochem.* **1986**, *30*, 123.

(18) Chini, P. *J. Organomet. Chem.* **1980**, *200*, 37.

(19) (a) Adams, R. D.; Cotton, F. A., Eds.; *Catalysis by Di- and Polynuclear Metal Cluster Complexes*; Wiley-VCH: New York, 1998. (b) Gates, B. C.; Guczi, L.; Knözinger, H., Eds.; *Metal Clusters in Catalysis*; Elsevier: Amsterdam, The Netherlands, 1986. (c) Shriver, D. F.; Kaesz, H. D.; Adams, R. D., Eds.; *The Chemistry of Metal Clusters Complexes*; VCH Publishers: New York, 1990.

(20) Adams, R. D.; Captain, B. *Acc. Chem. Res.* **2009**, *42*, 409.

(21) Budzelaar, P. H. M. *gNMR for Windows*, NMR Simulation Program (5.0.6.0); IvorySoft, Adept Scientific: Letchworth, U.K., 2006.

(22) (a) Brown, C.; Heaton, B. T.; Chini, P.; Fumagalli, A.; Longoni, G. *J. Chem. Soc., Dalton Trans.* **1977**, 309. (b) Brown, C.; Heaton, B. T.; Towl, A. D. C.; Chini, P.; Fumagalli, A.; Longoni, G. *J. Organomet. Chem.* **1979**, *181*, 233. (c) Pronk, B. J.; Brom, H.; Longoni, G.; Ceriotti, A. *Solid State Commun.* **1987**, *64*, 7.

(23) (a) Cordero, B.; Gómez, V.; Platero-Prats, A. E.; Revés, M.; Echevarría, J.; Cremades, E.; Barragán, F.; Alvarez, S. *Dalton Trans.* **2008**, 2832. (b) Bondi, A. *J. Phys. Chem.* **1964**, *68*, 441.

(24) Johnson, B. F. G.; McIndoe, J. S. *Coord. Chem. Rev.* **2000**, *200*–*202*, 901.

(25) Adams, R. D.; Captain, B. *Angew. Chem., Int. Ed.* **2008**, *47*, 252.

(26) (a) Gourdon, A.; Jeannin, Y. *J. Organomet. Chem.* **1992**, *440*, 353. (b) Zanello, P.; Laschi, F.; Cinquantini, A.; Della Pergola, R.; Garlaschelli, L.; Cucco, M.; Demartin, F.; Spalding, T. R. *Inorg. Chim. Acta* **1994**, *226*, 1.

(27) (a) Blum, T.; Brown, M. P.; Heaton, B. T.; Hor, A. S.; Iggo, J. A.; Sabounchei, J. S. Z.; Smith, A. K. *Dalton Trans.* **1994**, 513. (b) Sabounchei, J. S. Z.; Heaton, B. T.; Iggo, J. A.; Jacob, C.; Podkorytov, I. S. *J. Cluster Sci.* **2001**, *12*, 339.

(28) Bordoni, S.; Heaton, B. T.; Seregni, C.; Strona, L.; Goodfellow, R. J.; Hursthouse, M. B.; Thorhton-Pett, M.; Martinengo, S. *J. Chem. Soc., Dalton Trans.* **1988**, 2103.

(29) Della Pergola, R.; Garlaschelli, L.; Manassero, M.; Sansoni, M.; Strumolo, D. *J. Cluster Sci.* **2001**, *12*, 23.

(30) (a) Cifuentes, M. P.; Humphrey, M. G.; Wills, A. C. *J. Organomet. Chem.* **1996**, *513*, 85. (b) Cifuentes, M. P.; Humphrey, M. G.; Skelton, B. W.; White, A. H. *Organometallics* **1995**, *14*, 1536.

(31) (a) Albano, V. G.; Demartin, F.; Iapalucci, M. C.; Longoni, G.; Sironi, A.; Zanotti, V. *J. Chem. Soc., Chem. Commun.* **1990**, 547. (b) Albano, V. G.; Demartin, F.; Iapalucci, M. C.; Laschi, F.; Longoni, G.; Sironi, A.; Zanello, P. *J. Chem. Soc., Dalton Trans.* **1991**, 739. (c) Albano, V. G.; Demartin, F.; Femoni, C.; Iapalucci, M. C.; Longoni, G.; Monari, M.; Zanello, P. *J. Organomet. Chem.* **2000**, *593*–*594*, 325.

(32) Ceriotti, A.; Longoni, G.; Manassero, M.; Masciocchi, N.; Piro, G.; Resconi, L.; Sansoni, M. *J. Chem. Soc., Chem. Commun.* **1985**, 1402.

(33) Selvakanna, P. R.; Lampre, I.; Erard, M.; Remita, H. *J. Phys. Chem. C* **2008**, *112*, 18722.

(34) (a) Ichikawa, M. In *Metal Clusters in Chemistry*; Braunstein, P., Oro, L. A., Raithby, P. R., Eds.; Wiley-VCH: New York, 1999; p 1273. (b) Ichikawa, M. In *Chemisorption and Reactivity on Supported Clusters and Thin Films*; Lambert, R. M., Pacchioni; G. G., Eds.; Kluwer: Dordrecht, The Netherlands, 1997; p 153. (c) Paul, H.; Basu, S.; Bhaduri, S.; Lahiri, G. K. *J. Organomet. Chem.* **2004**, *689*, 309.

(35) (a) Maity, P.; Basu, S.; Bhaduri, S.; Lahiri, G. K. *J. Mol. Catal. A* **2007**, *270*, 117. (b) Gupta, N. S.; Basu, S.; Payra, P.; Mathur, P.; Bhaduri, S.; Lahiri, G. K. *Dalton Trans.* **2007**, 2594. (c) Maity, P.; Gopinath, S.; Bhaduri, S.; Lahiri, G. K. *Green Chem.* **2009**, *11*, 554.

(36) (a) Xie, J.; Zhang, Q.; Zhou, W.; Lee, J. Y.; Wang, D. I. C. *Langmuir* **2009**, *25*, 6454. (b) Fukuoka, A.; Higashimoto, N.; Sakamoto, Y.; Sasaki, M.; Sugimoto, N.; Inagaki, S.; Fukushima, Y.; Ichikawa, M. *Catal. Today* **2001**, *66*, 23. (c) Nováková, J.; Kubelková,

L.; Hülstede, P.; Jaeger, N. I.; Schulz-Ekloff, G. *J. Mol. Catal. A* **1996**, *111*, 123.
(37) Keller, E. *SCHAKAL99*; University of Freiburg: Freiburg, Germany, 1999.
(38) Sheldrick, G. M. *SADABS, Program for empirical absorption correction*; University of Göttingen: Göttingen, Germany, 1996.
(39) Sheldrick, G. M. *SHELX97, Program for crystal structure determination*; University of Göttingen: Göttingen, Germany, 1997.

dx.doi.org/10.1021/ic3025414 | *Inorg. Chem.* 2013, 52, 4384−4395